Z. Wu
Department of Mechanical Engineering,
University of Michigan,
Ann Arbor, MI 48109-2125
e-mail: wuzhen@umich.edu

R. L. Harne
Department of Mechanical Engineering,
University of Michigan,
Ann Arbor, MI 48109-2125

K. W. Wang
Department of Mechanical Engineering,
University of Michigan,
Ann Arbor, MI 48109-2125

Excitation-Induced Stability in a Bistable Duffing Oscillator: Analysis and Experiments

The excitation-induced stability (EIS) phenomenon in a harmonically excited bistable Duffing oscillator is studied in this paper. Criteria to predict system and excitation conditions necessary to maintain EIS are derived through a combination of the method of harmonic balance, perturbation theory, and stability theory for Mathieu's equation. Accuracy of the criteria is verified by analytical and numerical studies. We demonstrate that damping primarily determines the likelihood of attaining EIS response when several dynamics coexist while excitation level governs both the existence and frequency range of the EIS region, providing comprehensive guidance for realizing or avoiding EIS dynamics. Experimental results are in good agreement regarding the comprehensive influence of excitation conditions on the inducement of EIS. [DOI: 10.1115/1.4026974]

Keywords: bistable oscillator, excitation-induced stability, dynamic stabilization, Mathieu's equation

1 Introduction

For many years, the bistable Duffing oscillator has attracted considerable attention due to its rich dynamical behavior and numerous embodiments in mechanical, chemical, and engineering systems [1–11]. The double-well Duffing equation was derived, by a single mode approximation, as a mathematical model to describe the transverse deflection of a buckled beam [1]. Holmes [2] theoretically analyzed the chaotic dynamics of a bistable oscillator that is experimentally realized using a ferromagnetic cantilever beam deflected from a central position by a surrounding pair of attractive magnetic fields [3,4]. Since then, great focus has been put toward understanding and characterizing the onset of chaotic dynamics of double-well systems [5–8]. In parallel with the extensive research on "strange" behaviors of bistable systems, a number of researchers have studied the steady-state harmonic responses. Tseng and Dugundji [9] analytically and experimentally considered intrawell (low-energy orbit) and regular interwell (high-energy orbit) dynamics of a buckled beam with clamped ends and determined the "snap-through" threshold. Szemplińska-Stupnicka and Rudowski [10] generalized these results by providing approximate closed-form criteria for intrawell and regular interwell oscillations and for cross-well chaos. Harne et al. [11]. recently proposed a set of straightforward conditions that govern interwell responses in the context of bistable vibration energy harvesting systems.

Holmes [2] demonstrated that when forcing level exceeds a threshold value, the unstable saddle fixed point on the Poincaré map could stabilize itself through a pitchfork bifurcation. Such dynamic stabilization or excitation-induced stability (EIS) is commonly observed for systems under parametric excitation [12]. A classic system that may exhibit EIS is the parametrically-forced pendulum [13–15]. Comparatively fewer studies have focused on EIS in a double-well Duffing system. Blair et al. [16]. documented the phenomenon on a forced bistable Duffing oscillator that was later experimentally demonstrated by analog circuit studies through bifurcation analysis by Kim et al. [17,18]. Recent studies in vibration energy harvesting [19,20] and vibration control [21] also observed similar dynamical behaviors on single or two degree-of-freedom systems including bistable members. Since both regular interwell and EIS dynamics are oscillations around the unstable equilibrium position, criteria governing inducement of EIS are valuable for preferred utilization of a bistable Duffing oscillator, which models many real-world systems.

Despite the importance, explicit criteria that determine system and excitation parameters defining the EIS region remain unreported and validation of such criteria through experimental investigations with mechanical bistable systems are outstanding. Validation through experimentation with *mechanical* oscillators is important to demonstrate their utility for the many structural and engineered bistable systems, surveyed above. On the one hand, for applications that benefit from large amplitude regular interwell responses like vibration energy harvesting [22,23], criteria may provide guidance to design the bistable oscillator to avoid activation of EIS dynamics. On the other hand, for systems that require low dynamic stiffness like vibration isolation [24], following the criteria can help sustain small amplitude EIS response and preserve system integrity.

Hence, to provide guiding principles in realizing or avoiding EIS dynamics, the present paper aims to complement previous work by deriving criteria to predict the existence and sustainable range of EIS for a bistable Duffing oscillator. First, a perturbation to steady-state response solutions is applied that results in a Mathieu's equation. The criteria are then determined by combining the stability theory of Mathieu's equation and closed-form expression of steady-state response. The influences of key parameters on the inducement of EIS dynamics are investigated. Analytical findings on system dependence on excitation conditions are experimentally validated using a classical bistable mechanical system: the buckled ferromagnetic cantilever beam.

2 Mathematical Formulation

2.1 Governing Equation. The nondimensional governing equation of a harmonically excited bistable Duffing oscillator may be written as

$$\ddot{x} + \gamma\dot{x} - x + x^3 = p\cos(\omega t) \tag{1}$$

where x is the normalized relative displacement between an inertial frame and the oscillator mass as measured from the central unstable equilibrium, γ is the damping factor, p is the excitation

Manuscript received September 10, 2013; final manuscript received February 27, 2014; published online October 14, 2014. Assoc. Editor: D. Dane Quinn.

level, and the operator $(\dot{})$ represents the derivative with respect to nondimensional time t. Previous studies [9,11,20,25] indicate that the most fundamental, periodic vibration of a bistable oscillator can be captured by a single term Fourier expansion $x(t) = c(t) + r(t)\cos(\omega t - \phi(t))$. The offset term $c(t)$ is selected as zero or nonzero based on whether the dynamics of interest are intrawell (oscillations orbiting a stable equilibrium position) or interwell (oscillations crossing the unstable equilibrium position twice per excitation period). Therefore, the symmetry of the response about the unstable equilibrium serves as an important criterion to distinguish the dynamical responses. Substituting the expression for $x(t)$ into Eq. (1), assuming slow-varying coefficients, and eliminating higher-order terms, the steady-state vibration amplitude r satisfies [11,26]

$$\frac{9}{16}r^6 - \frac{3}{2}(1+\omega^2)r^4 + \left[(1+\omega^2)^2 + (\gamma\omega)^2\right]r^2 = p^2 \tag{2}$$

or

$$\frac{225}{16}r^6 - \frac{3}{2}(1+\omega^2)r^4 + \left[(1+\omega^2)^2 + (\gamma\omega)^2\right]r^2 = p^2 \tag{3}$$

where Eqs. (2) and (3) govern the vibration amplitude of interwell and intrawell dynamics, respectively.

2.2 Stability Analysis. Since EIS dynamics represent oscillations crossing the unstable equilibrium position twice per excitation period [17,18], such phenomena are classified as a form of interwell response. Detailed stability analysis on intrawell dynamics for Eq. (3) is omitted here for brevity. To determine the stability of the interwell response, a perturbation $y(t)$ is applied to the steady-state response $x_{ss} = r\cos(\omega t - \Phi)$, where r is the steady-state response amplitude determined from Eq. (2). Substituting the expression $x(t) = x_{ss}(t) + y(t)$ into Eq. (1) and neglecting higher order terms of $y(t)$, the resulting dynamical equation for perturbation $y(t)$ becomes

$$\ddot{y} + \gamma\dot{y} + \left[\left(\frac{3r^2}{2} - 1\right) + \frac{3r^2}{2}\cos(2\omega t - 2\Phi)\right]y = 0 \tag{4}$$

Stability of the interwell response can therefore be determined from the stability of perturbation $y(t)$; stable perturbation $y(t)$ corresponds to a stable steady-state response r and vice versa. To better analyze the stability of $y(t)$, Eq. (4) is first expressed as

$$y'' + \frac{\gamma}{2\omega}y' + \left(\frac{\alpha}{4\omega^2} + \frac{\beta}{4\omega^2}\cos(T)\right)y = 0 \tag{5}$$

with $T = 2\omega t - 2\Phi, \alpha = 3r^2/2 - 1, \beta = 3r^2/2$ and operator $()'$ represents the derivative with respect to time T. Applying a change of variable $\varphi = y\exp(\frac{1}{2}\int_0^T(\gamma/2\omega)ds)$ [27], Eq. (5) is transformed into a standard Mathieu's form

$$\varphi'' + (\delta + \varepsilon\cos(T))\varphi = 0 \tag{6}$$

where the terms are defined as

$$\delta = \alpha/4\omega^2 - \gamma^2/16\omega^2; \quad \varepsilon = \beta/4\omega^2$$

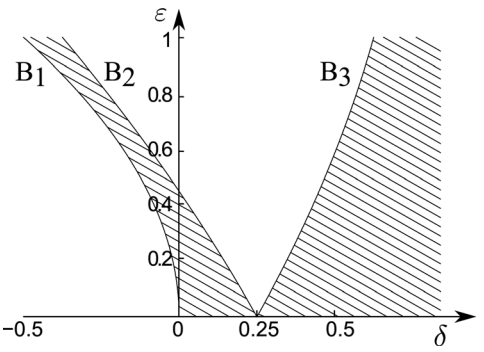

Fig. 1 Schematic of Mathieu's resonance tongue. Hatched areas correspond to stable domains of Mathieu's equation. B_1, B_2, and B_3 are the first three transition curves on the $\delta-\varepsilon$ plane.

Hence, stability can be determined from the Mathieu's resonance tongue boundaries, schematically shown in Fig. 1 with hatched areas corresponding to stable domains for Eq. (6), which are specifically explored in this work. Applying the Poincaré–Lindstedt method [28,29], the three lowest-order transition curves labeled B_1, B_2, and B_3 may be approximated as

$$\begin{aligned} &B_1: \delta = -\frac{1}{2}\varepsilon^2 + O(\varepsilon^4); \quad B_2: \delta = \frac{1}{4} - \frac{1}{2}\varepsilon - \frac{1}{8}\varepsilon^2 + O(\varepsilon^3); \\ &B_3: \delta = \frac{1}{4} + \frac{1}{2}\varepsilon - \frac{1}{8}\varepsilon^2 + O(\varepsilon^3) \end{aligned} \tag{7}$$

Therefore, from Fig. 1 the perturbation φ is stable if δ is between B_1 and B_2 or above B_3, i.e., if

$$-\frac{1}{2}\varepsilon^2 < \delta < \frac{1}{4} - \frac{1}{2}\varepsilon - \frac{1}{8}\varepsilon^2; \delta > \frac{1}{4} + \frac{1}{2}\varepsilon - \frac{1}{8}\varepsilon^2 \tag{8}$$

Neglecting terms ε of order 2 or higher in Eq. (8) and substituting expressions for δ and ε defined in Eq. (6), the steady-state response r is stable if

$$S_1 < r < S_2; \quad r > S_3 \tag{9}$$

where

$$\begin{aligned} &S_1 = \sqrt{(4+\gamma^2)/6}; \quad S_2 = \sqrt{(4+\gamma^2+4\omega^2)/9}; \\ &S_3 = \sqrt{(4+\gamma^2+4\omega^2)/3} \end{aligned}$$

The three boundaries in Eq. (9) expressed in terms of system parameters p, γ, and excitation frequency ω are criteria to determine the stability of the interwell response for a bistable Duffing oscillator. Vibration bounded by curves S_1 and S_2 is the EIS response. The intersections of the steady-state response amplitude curve $r(\gamma, p, \omega)$, determined from the roots of Eq. (2), and the three transition curves, respectively, govern the frequencies at which interwell dynamics change stability. For instance, the upper frequency bound for EIS, at which responses transition between interwell and intrawell dynamics is determined by substituting $r = S_1$ into Eq. (2), and the resulting expression is

$$\omega_{Ub} = \sqrt{\frac{-16 - 16\gamma^2 - 3\gamma^4 + 2\sqrt{2}\sqrt{192p^2 + 64\gamma^2 + 48p^2\gamma^2 + 48\gamma^4 + 12\gamma^6 + \gamma^8}}{8(4+\gamma^2)}} \tag{10}$$

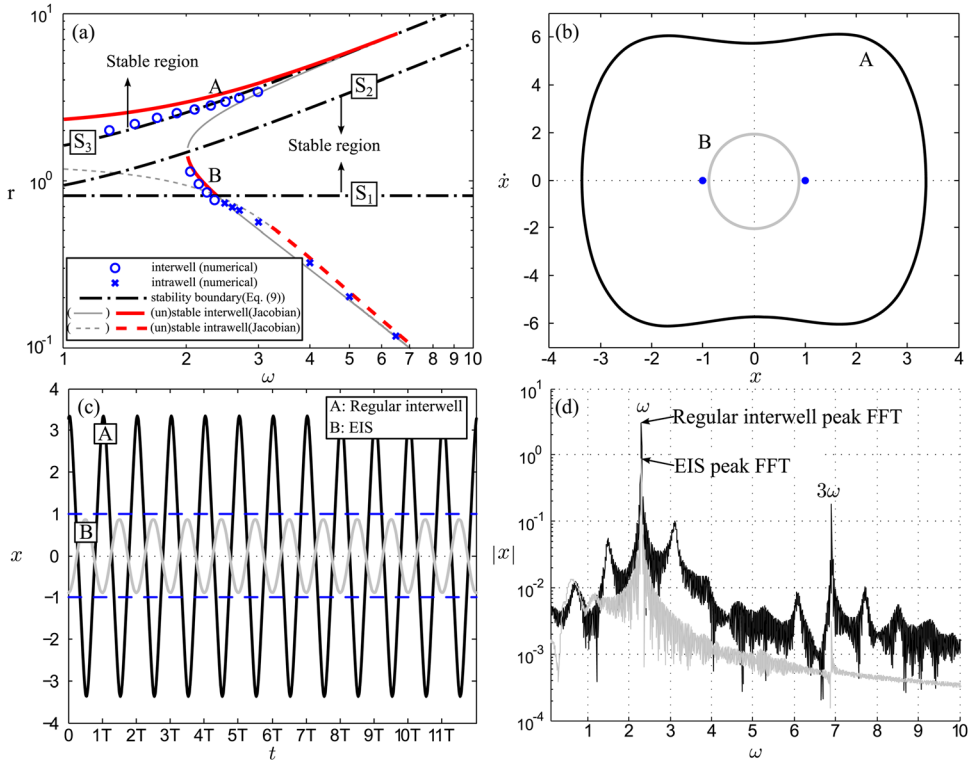

Fig. 2 (*a*) Steady-state response amplitude. Red solid (dashed) lines are stable interwell (intrawell) responses whose stability are determined via Jacobian analysis; black dashed dotted lines are the first three approximated transition curves determined from Mathieu's resonance tongue. Blue circles (crosses) correspond to interwell (intrawell) responses computed via direct numerical integration. Gray lines are analytically predicted unstable responses. Criteria predict stable interwell response regions between S_1 and S_2 or above S_3 (as indicated by arrows). Two interwell responses A and B coexist at $\omega = 2.3$. Corresponding (*b*) phase portrait, (*c*) time series, and (*d*) frequency spectra are presented, with black and gray representing regular interwell and EIS, respectively. Blue dashed lines (dots) indicate the positions of the stable equilibria.

which can be simplified into $\omega_{Ub} = \sqrt{(\sqrt{6}p - 1)/2}$ assuming small damping $\gamma \ll 1$. Likewise, the frequency at which regular large amplitude interwell response becomes unstable is determined by replacing r with S_3 in Eq. (2) and the resulting expression is

$$\omega_{\text{inter}} = \sqrt{\frac{-\gamma^2 + \sqrt{3p^2\gamma^2 + \gamma^4}}{2\gamma^2}} \tag{11}$$

By the same token, the lower frequency bound of EIS ω_{Lb}, which separates the regular interwell and EIS dynamics, determined by combining S_2 and Eq. (2), satisfies

$$\frac{1}{9}\left(4 + \gamma^2 + 4\omega_{Lb}^2\right)\left[\gamma^2\omega_{Lb}^2 + \left(-\frac{2}{3} - 2\omega_{Lb}^2/3 + \gamma^2/12\right)^2\right] = p^2 \tag{12}$$

which is a cubic characteristic polynomial of variable ω_{Lb}^2. With small damping assumption, the expression can be simplified as $\omega_{Lb} = \sqrt{-1 + (3/2)^{4/3}p^{2/3}}$.

Lastly, the minimum forcing level p_{cr}. required to maintain EIS is determined by equating S_1 and S_2. This is identical to equating the lower frequency ω_{Lb} and upper frequency ω_{Ub} bounds defined in Eqs. (10) and (12). Substituting the resulting frequency ω into Eq. (2) yields an expression for critical forcing level

$$p_{\text{cr}} = \frac{\sqrt{32 + 24\gamma^2 + 8\gamma^4 + \gamma^6}}{4\sqrt{3}} \tag{13}$$

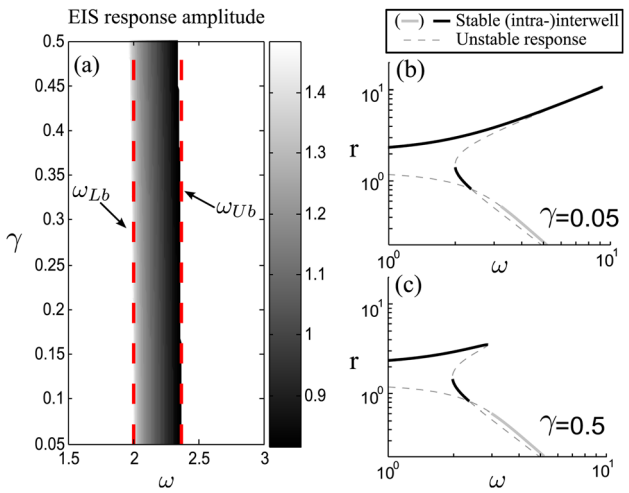

Fig. 3 (*a*) EIS response amplitude as a function of damping and frequency with system parameter $p = 5$. Increasing lightness of the contour represents increasing response amplitude. Dashed lines correspond to estimated frequency boundaries using simplified form of Eqs. (10) and (12). (*b*) and (*c*) are two representative responses with damping $\gamma = 0.05$ and $\gamma = 0.5$. Solid black (gray) lines indicate interwell (intrawell) responses and dashed gray lines are analytically determined unstable responses.

Similarly, Eq. (13) can be further simplified into $p_{cr} = \sqrt{2/3}$ for small damping γ.

3 Analytical and Experimental Investigations

3.1 Stability Criteria Validation. In this section, we verify the accuracy of stability boundaries developed in Sec. 2.2. For comparison, stability of the steady-state response approximated via the one-term harmonic balance method is determined by Jacobian analysis [20,26]. Direct numerical integration results are also provided. Figure 2(*a*) presents the response amplitude of both interwell and intrawell vibration with system parameters $p = 5$ and $\gamma = 0.1$. Dash–dot lines represent the approximated stability transition criteria for interwell response obtained from Eq. (9), solid (dashed) lines correspond to interwell (intrawell) response via the combination of harmonic balance and Jacobian analysis, and circles (crosses) are interwell (intrawell) vibration amplitudes determined from direct numerical integration.

To exemplify the characteristic responses of the two interwell dynamic forms, representative points A and B are taken from Fig. 2(*a*) at $\omega = 2.3$, where regular interwell (point A) and EIS (point B) responses coexist. Figures 2(*b*)–2(*d*) depict the corresponding phase portrait, time domain, and frequency spectra of the responses, where black and gray curves represent regular interwell and EIS, respectively. Dots in Fig. 2(*b*) and dashed lines in Fig. 2(*c*) represent stable equilibrium positions. As indicated in Figs. 2(*b*) and 2(*c*), both responses are symmetric about the central unstable equilibrium, which is the defining characteristic of an interwell response, as compared to intrawell. However, apart from this, the regular high-orbit interwell and EIS behaviors are vastly different from each other. First, regular high-orbit interwell response has a much greater vibration amplitude. Next, Fig. 2(*c*) demonstrates that the responses are almost out-of phase with each other, implying a phase transition between two different interwell responses [12,20]. As shown through both the phase portrait and time series, the EIS response is also near sinusoidal in contrast to the regular interwell vibration which includes other prominent spectral components, verified by the notable spectral content at 3ω for the regular interwell response in Fig. 2(*d*).

Since Jacobian analysis does not rely on approximation to determine the stability of the response, it serves as a viable benchmark against which the approximated stability criteria derived from Eq. (9) are compared, to verify their accuracy. In Fig. 2(*a*), the criteria predict steady-state regular interwell response amplitude satisfying $r > S_3$ to be stable (indicated by the arrow), which coincides with stability limits determined via Jacobian analysis

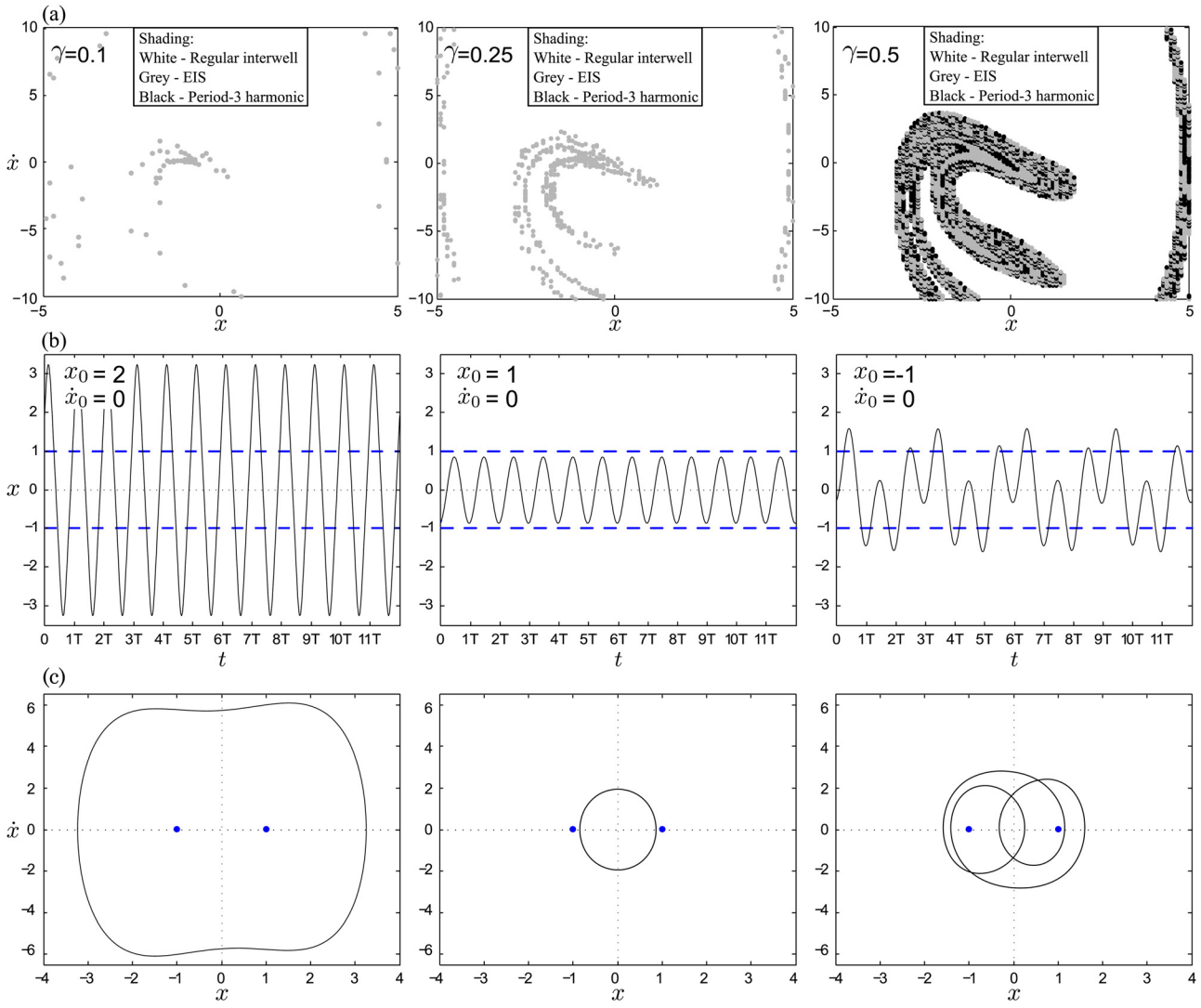

Fig. 4 (*a*) Basin of attraction map for system parameters $p = 5$, $\omega = 2.3$ with white, gray, and black shading representing regular interwell response, EIS, and period-3 harmonic interwell responses, respectively. (*b*) Steady-state time domain responses ($T = 2\pi/\omega$) and (*c*) corresponding phase portraits for different initial conditions with damping $\gamma = 0.5$. In (*b*) and (*c*) blue dashed lines and dots, respectively, represent positions of two stable equilibria.

and is in good agreement with numerically predicted responses. The criteria satisfying $S_1 < r < S_2$ predict stable EIS from $\omega \approx 2$ to $\omega \approx 2.37$, which is also in good agreement to numerical results and Jacobian analysis, further validating the accuracy of the approximated stability criteria.

3.2 Effect of Damping γ. To investigate the influence of damping, responses were determined using system characteristics $p = 5$ and damping γ ranging from 0.05 to 0.5. Figure 3(*a*) presents the EIS response amplitude as a function of damping and input frequency, determined from the stable bandwidth predicted by harmonic balance and Jacobian analysis. Increasing lightness of the contour represents increasing response amplitude. Both approximated upper and lower frequency bounds (ω_{Lb} and ω_{Ub}), determined using simplified form of Eqs. (10) and (12), are presented as red dashed lines.

As damping γ changes from 0.05 to 0.5, analysis predicts EIS will exist while its frequency range of stability shifts slightly downward. However, as damping changes, the predicted steady-state response amplitude does not alter to any significant degree for a given excitation frequency, indicating that damping has little influence on the stability and vibration amplitude of the EIS dynamic. Nonetheless, a drastic degradation on the bandwidth of stable regular large amplitude interwell response is observed as damping γ increases. Figures 3(*b*) and 3(*c*) depict representative response amplitudes, determined from Eqs. (2) and (3); solid black (gray) lines represent interwell (intrawell) responses and dashed gray lines denote analytically determined unstable responses. For damping $\gamma = 0.05$, Fig. 3(*b*), analysis predicts the regular interwell branch is destabilized for excitation frequencies $\omega > 9.27$, whereas the response destabilizes for frequencies $\omega > 2.86$ for damping $\gamma = 0.5$, Fig. 3(*c*). Overall, the criteria boundary definitions (red dashed curves) and analytically determined boundaries (contour limits) are in good agreement for smaller values of damping γ.

For the system parameters under study, EIS always coexists with the regular interwell response, as depicted in Figs. 3(*b*) and 3(*c*). To determine which outcome is more likely as a consequence to changing initial conditions, the basins of attraction are investigated at an excitation frequency $\omega = 2.3$ and level $p = 5$. Figure 4(*a*) shows numerically determined basins for damping $\gamma = [0.1, 0.25, 0.5]$. Three distinct responses are observed. In Fig. 4(*a*), white (unshaded) corresponds to regular interwell, gray shading indicates EIS, and black shading represents period-3 harmonic interwell response. As damping increases from $\gamma = 0.1$ to $\gamma = 0.25$, a greater number of initial conditions leads to EIS. For the highest damping considered $\gamma = 0.5$, period-3 harmonic interwell response is induced, appearing to primarily coalesce in a fractal manner among the initial conditions leading to EIS. The three dynamic responses are illustrated in Figs. 4(*b*) and 4(*c*) showing steady-state time-series and phase portraits, respectively, for initial conditions (2,0), (1,0), and (−1,0) and damping $\gamma = 0.5$. Figure 4 exemplifies the initial condition and damping dependence of either obtaining or avoiding EIS phenomena. For applications hoping to realize EIS response like dynamic structural stabilization, the need for high damping and strict control over initial conditions indicates a less favorable opportunity that EIS may be harnessed. In contrast, for applications where EIS is a detriment to performance like vibration energy harvesting, Fig. 4 highlights that lighter damping and relative independence of initial conditions helps maintain the advantageous regular interwell dynamics.

3.3 Effect of Excitation Level p. The influence of excitation level $0.1 \le p \le 15$ is evaluated while damping $\gamma = 0.1$. Figure 5 presents the EIS response amplitude as a function of excitation level and frequency. The contour in Fig. 5(*a*) shows that, for a given excitation level, the amplitude of the EIS response is decreasing as a consequence to increasing excitation frequency.

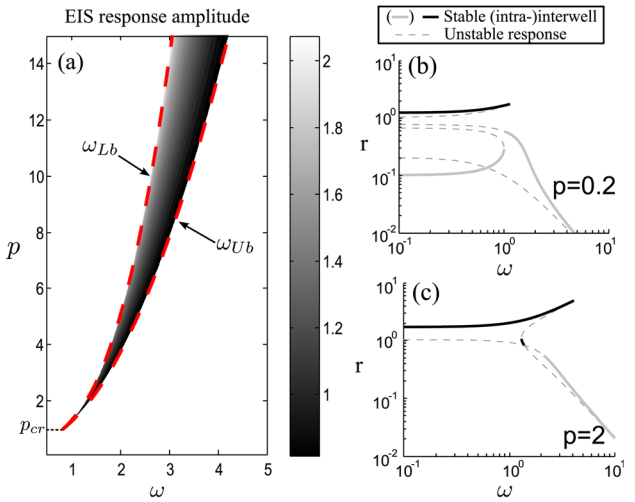

Fig. 5 (*a*) EIS response amplitude as a function of excitation level and frequency with system parameter $\gamma = 0.1$. Increasing lightness of the contour represents increasing in response amplitude. Dashed lines correspond to estimated frequency boundaries using simplified form of Eqs. (10) and (12). (*b*) and (*c*) are two representative responses with excitation level $p = 0.2$ and $p = 2$. Solid black (gray) lines indicate interwell (intrawell) responses and dashed gray lines are analytically determined unstable responses.

Both frequency bounds (ω_{Lb} and ω_{Ub}) determined from the criteria of Eqs. (10) and (12) match very well with the limits of EIS response predicted by harmonic balance and Jacobian analysis. When excitation level p is less than critical value p_{cr}, determined from Eq. (13), no stable EIS region exists. This is verified by the corresponding response predictions from the harmonic balance method, Fig. 5(*b*). As p increases above the threshold value, Fig. 5(*a*) show that the frequency range of EIS responses correspondingly increases. The harmonic balance response predictions in Fig. 5(*c*) show that the EIS branch indeed materializes for an excitation level above the threshold value p_{cr}. These results help verify the criteria's accuracy in governing EIS response existence and stability and the relative importance of excitation parameters.

To further validate the roles of excitation conditions on the inducement of EIS response, experiments on a ferromagnetic bistable cantilever beam are conducted. A schematic and photograph of the experimental setup are provided in Fig. 6. A supporting structural frame, from which the beam is cantilevered, is attached to an electrodynamic shaker table activated in the direction indicated in Fig. 6. Motion of the beam tip x is the response

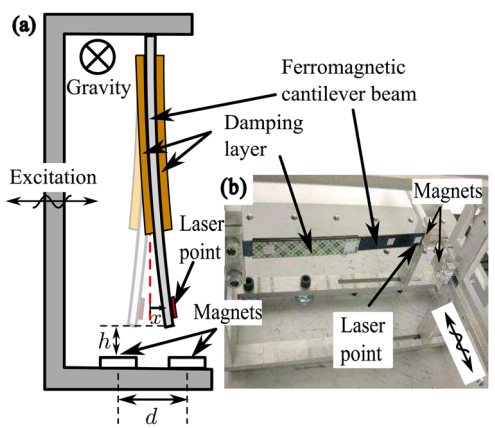

Fig. 6 (*a*) Schematic of experimental test setup. (*b*) Photograph of test setup.

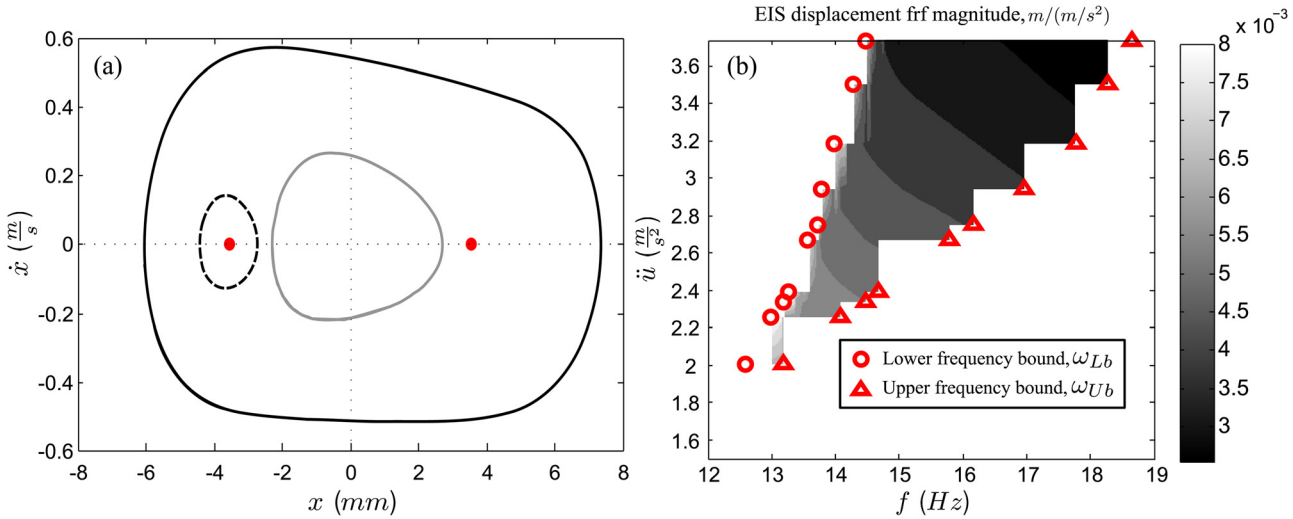

Fig. 7 (*a*) Experimentally determined phase portraits with dashed black, solid gray, and black representing intrawell, EIS, and regular interwell responses, respectively. Two dots represent two stable equilibrium positions of the bistable oscillator. (*b*) Experimentally determined displacement frf of the bistable oscillator as a function of shaker input frequency and amplitude. Circles and triangles are experimentally determined frequency boundaries of the stable EIS region.

coordinate of interest. Bistability of the beam deflection is generated using attractive magnetic fields [4]. A 0.05 cm thick and 1.27 cm wide spring steel beam is clamped with a cantilevered length of 14.0 cm. Two 0.64 cm thick magnets of diameter 1.27 cm are placed d =2.54 cm apart from center to center to realize a double-well potential. At rest, the normal distance between tip of the beam and magnet is approximately h =0.8 cm. To better attain EIS phenomena as suggested in Sec. 3.2, the beam damping is increased, here by applying a dissipative tape along the beam length undergoing greatest strain, assuming the dynamic buckling response is the fundamental mode. In this configuration when excited by low level white noise, the fundamental resonance frequency of the buckled beam around each magnet is approximately 19.5 Hz and the damping loss factor is identified to be $\gamma \approx 0.16$. Acceleration of the harmonic shaker excitation and displacement of the cantilever beam tip are recorded.

The shaker supplies a backward-swept sinusoid (−0.05 Hz/s) such that the beam response is measured in the bandwidth of 12–24 Hz. The upper frequency bound ω_{Ub} is based on whether the oscillation is around one of the stable equilibria or the unstable equilibrium. For small oscillations, this characteristic change determines the transition between intrawell and the EIS response. The lower frequency bound ω_{Lb} is identified depending on the response amplitude. A sudden increase in amplitude is the transition from EIS to regular high orbit interwell during the backward frequency sweep. Figure 7(*a*) plots experimentally recorded phase portraits for intrawell, EIS, and regular interwell dynamics. The regular interwell and EIS responses oscillate nearly symmetrical about the unstable equilibrium, while intrawell response only encircles one of the stable equilibrium. The displacement frequency response function (frf) magnitude of the EIS response is presented as the contour in Fig. 7(*b*) for varying shaker input frequency f and excitation level $\ddot{u}$. The frf is determined as the ratio of relative cantilever beam tip displacement and the shaker acceleration. The contour plot represents increasing displacement frf magnitude by increasing lightness of shading. The sweep tests are conducted for average base acceleration ranging from 2 to 3.74 m/s^2. The frequency range of EIS responses is presented in Fig. 7(*b*) by the distance spanning two boundary points for a given excitation level. The bandwidth is seen to increase as excitation level increases, corresponding well with the trend predicted analytical as shown in Fig. 5. Experimental measurements also corroborate the analytical finding that EIS response amplitudes for a given excitation level decrease as excitation frequency increases. Overall, the results of the experiments are in very good qualitative agreement with the analytical studies and demonstrate the prominent role of excitations in the realization and characteristics of EIS for a bistable Duffing oscillator.

4 Conclusion

This paper presented analytical and experimental studies on the excitation-induced stability phenomenon of a bistable Duffing oscillator. Criteria are derived that determine the critical forcing level to induce EIS dynamics and the frequency range across which EIS occurs. The existence and frequency range of EIS responses are shown to be primarily influenced by excitation level; for levels greater than the critical threshold the frequency range of EIS steadily increases. It is also shown that damping has little effect on the existence and frequency range of EIS, although an increase in damping increases the likelihood of obtaining an EIS response when multiple dynamics coexist. These findings are corroborated through simulation. The corresponding experimental results are also in good agreement with the key trends, demonstrating the accuracy of the derived criteria. The results of this work provide effective guidance in realizing or avoiding EIS dynamics for a bistable Duffing system.

References

[1] Bolotin, V. V., 1964, *The Dynamic Stability of Elastic Systems*, Holden Day, San Francisco.

[2] Holmes, P., 1979, "A Nonlinear Oscillator With a Strange Attractor," Philos. Trans. R. Soc. London, **292**(1394), pp. 419–448.

[3] Moon, F. C., and Holmes, P. J., 1979, "A Magnetoelastic Strange Attractor," J. Sound Vib., **65**(2), pp. 275–296.

[4] Moon, F. C., 1980, "Experiments on Chaotic Motions of a Forced Nonlinear Oscillator: Strange Attractors," ASME J. Appl. Mech., **47**(3), pp. 638–644.

[5] Dowell, E. H., and Pezeshki, C., 1986, "On the Understanding of Chaos in Duffings Equation Including a Comparison With Experiment," ASME J. Appl. Mech., **53**(1), pp. 5–9.

[6] Tang, D. M., and Dowell, E. H., 1988, "On the Threshold Force for Chaotic Motions for a Forced Buckled Beam," ASME J. Appl. Mech., **55**(1), pp. 190–196.

[7] Szemplińska-Stupnicka, W., and Rudowski, J., 1992, "Local Methods in Predicting Occurrence of Chaos in Two-Well Potential Systems: Superharmonic Frequency Region," J. Sound Vib., **152**(1), pp. 57–72.

[8] Stanton, S. C., Mann, B. P., and Owens, B. A. M., 2012, "Melnikov Theoretic Methods for Characterizing the Dynamics of the Bistable Piezoelectric Inertial Generator in Complex Spectral Environments," Physica D, **241**(6), pp. 711–720.

[9] Tseng, W.-Y., and Dugundji, J., 1971, "Nonlinear Vibrations of a Buckled Beam Under Harmonic Excitation," ASME J. Appl. Mech., **38**(2), pp. 467–476.

[10] Szemplińska-Stupnicka, W., and Rudowski, J., 1993, "Steady States in the Twin-Well Potential Oscillator: Computer Simulations and Approximate Analytical Studies," Chaos, **3**(3), pp. 375–385.
[11] Harne, R. L., Thota, M., and Wang, K. W., 2013, "Concise and High-Fidelity Predictive Criteria for Maximizing Performance and Robustness of Bistable Energy Harvesters," Appl. Phys. Lett., **102**(5), p. 053903.
[12] Ibrahim, R. A., 2006, "Excitation-Induced Stability and Phase Transition: A Review," J. Vib. Control, **12**(10), pp. 1093–1170.
[13] Blackburn, J. A., Smith, H. J. T., and Grønbech-Jensen, N., 1992, "Stability and Hopf Bifurcations in an Inverted Pendulum," Am. J. Phys., **60**(10), pp. 903–908.
[14] Butikov, E. I., 2001, "On the Dynamic Stabilization of an Inverted Pendulum," Am. J. Phys., **69**(7), pp. 755–768.
[15] Seyranian, A. A., and Seyranian, A. P., 2006, "The Stability of an Inverted Pendulum With a Vibrating Suspension Point," J. Appl. Math. Mech., **70**(5), pp. 754–761.
[16] Blair, K. B., Krousgrill, C. M., and Farris, T. N., 1997, "Harmonic Balance and Continuation Techniques in the Dynamic Analysis of Duffing's Equation," J. Sound Vib., **202**(5), pp. 717–731.
[17] Kim, S.-Y., and Kim, Y., 2000, "Dynamic Stabilization in the Double-Well Duffing Oscillator," Phys. Rev. E, **61**(6), pp. 6517–6520.
[18] Kim, Y., Lee, S. Y., and Kim, S.-Y., 2000, "Experimental Observation of Dynamic Stabilization in a Double-Well Duffing Oscillator," Phys. Lett. A, **275**(4), pp. 254–259.
[19] Karami, M. A., and Inman, D. J., 2011, "Equivalent Damping and Frequency Change for Linear and Nonlinear Hybrid Vibrational Energy Harvesting Systems," J. Sound Vib., **330**(23), pp. 5583–5597.
[20] Wu, Z., Harne, R. L., and Wang, K. W., 2014, "Energy Harvester Synthesis Via Coupled Linear-Bistable System With Multistable Dynamics," ASME J. Appl. Mech., **81**(6), p. 061005.
[21] Johnson, D. R., Harne, R. L., and Wang, K. W., 2013, "A Disturbance Cancellation Perspective on Vibration Control Using a Bistable Snap Through Attachment," ASME J. Vib. Acoust. (accepted).
[22] Harne, R. L., and Wang, K. W., 2013, "A Review of the Recent Research on Vibration Energy Harvesting via Bistable Systems," Smart Mater. Struct., **22**(2), p. 023001.
[23] Masana, R., and Daqaq, M. F., 2011, "Relative Performance of a Vibratory Energy Harvester in Mono- and Bi-Stable Potentials," J. Sound Vib., **330**(24), pp. 6036–6052.
[24] Ibrahim, R. A., 2008, "Recent Advances in Nonlinear Passive Vibration Isolators," J. Sound Vib., **314**(3–5), pp. 371–452.
[25] Friswell, M. I., and Penny, J. E. T., 1994, "The Accuracy of Jump Frequencies in Series Solutions of the Response of a Duffing Oscillator," J. Sound Vib., **169**(2), pp. 261–269.
[26] Stanton, S. C., Owens, B. A. M., and Mann, B. P., 2012, "Harmonic Balance Analysis of the Bistable Piezoelectric Inertial Generator," J. Sound Vib., **331**(15), pp. 3617–3627.
[27] Gunderson, H., Rigas, H., and VanVleck, F. S., 1974, "A Technique for Determining Stability Regions for the Damped Mathieu Equation," SIAM J. Appl. Math., **26**(2), pp. 345–349.
[28] Jordan, D. W., and Smith, P., 2007, *Nonlinear Ordinary Differential Equations*, 4th ed., Oxford University Press, New York.
[29] Nayfeh, A. H., and Mook, D. T., 1979, *Nonlinear Oscillations*, John Wiley, New York.